Isolated hybrid normal/superconducting ring in a magnetic flux: From persistent current to Josephson current

Jérôme Cayssol,[1] Takis Kontos,[2] and Gilles Montambaux[1]
[1]*Laboratoire de Physique des Solides, Associé au CNRS, Université Paris Sud, 91405 Orsay, France*
[2]*CSNSM, CNRS, Université Paris Sud, 91405 Orsay, France*
(Received 10 June 2002; revised manuscript received 20 November 2002; published 8 May 2003)

We investigate the ground state current of an isolated hybrid normal/superconducting ring (NS ring), threaded by an Aharonov-Bohm magnetic flux. We calculate the excitation spectrum of the ring for any values of the lengths of the normal metal and of the superconductor. We describe the nonlinear flux dependence of the energy levels above and below the gap edge. Using a harmonics expansion for the current, we isolate the contribution due to these nonlinearities and we show that it vanishes for a large normal segment length d_N. The remaining contribution is very easy to evaluate from the linearized low energy spectrum. This decomposition allows us to recover in a controlled way the current-flux relationships for SNS junctions and for NS rings. We also study the crossover from persistent current to Josephson current in a multichannel NS ring at finite temperature.

DOI: 10.1103/PhysRevB.67.184508 PACS number(s): 74.45.+c, 73.23.−b

I. INTRODUCTION

In spite of the great amount of work devoted to this problem, a full understanding of the physics of persistent currents in normal mesoscopic rings is still lacking. On the other hand, the physics of the proximity effect in hybrid normal-superconducting mesoscopic structures has gained renewed interest recently due to progress in nanofabrication techniques. What is the interplay between these two phenomena? In order to address this question, we study a mesoscopic isolated normal/superconducting loop (NS loop) made of a normal metal of length d_N and a superconductor of length d_S as depicted in Fig. 1. This NS ring is mesoscopic in the sense that the normal segment is shorter than the coherence length L_ϕ. As a consequence of phase coherence, a nondissipative current flows in the ring when a magnetic flux ϕ is applied. In the absence of a superconductor, i.e., for the normal ring, this is the so-called persistent current which has the periodicity $\phi_0 = h/e$. When the superconducting segment is longer than its superconducting coherence length ξ_o, this current is analogous to the Josephson current in SNS junctions, with a periodicity $h/2e$.

Büttiker and Klapwijk[1] (BK) showed that the physical mechanism responsible for the crossover between these two cases is the tunneling of Andreev quasiparticules[2] through the superconducting segment when its length d_S becomes of order ξ_o. However, BK studied only the low energy spectrum where energy levels vary linearly with the flux. They constructed the current-flux relationship $I(\phi)$ in analogy to that of long SNS junctions. In the present paper, we investigate the full NS loop spectrum. In particular, we describe carefully nonlinear variations of the level positions with the flux which appear both below and above the gap edge. Then, we address the question of a proper calculation of the current $I(\phi)$ which includes these new spectral features. The standard difficulty is to compute the sum of many single level currents $-\partial\epsilon/\partial\phi$ which are of the same order of magnitude and alternate in sign. In our approach, each harmonic of the total current $I(\phi)$ is expressed as the sum of a term proportional to a single level current at zero energy $-\partial\epsilon/\partial\phi(\epsilon = 0)$ plus an integral of the "curvature" $-\partial^2\epsilon/\partial^2\phi$ over the whole spectrum. For a long normal segment $d_N \gtrsim 2\xi_o$, the latter term is negligible and the current $I(\phi)$ can be obtained simply from the low energy linearized spectrum. In this limit, one recovers the BK result. For a short normal segment $d_N \lesssim 2\xi_o$, the curvature term leads to important deviations from the BK result. As a byproduct, one recovers the result for the long SNS junction when $d_S \to \infty$ and for the normal ring when $d_S \to 0$. This derivation of $I(\phi)$ for long SNS junctions is surprisingly simple compared to the original derivation of Refs. 3–5. These authors found that $I(\phi)$ is triangular, but disagreed with the value of the critical current. The simplicity of our approach enables us to show that Bardeen and Johnson[3] found the correct critical current for long SNS junctions. Beside the simplicity of the derivation, our decomposition gives us the possibility to control the approximation since the "curvature" term is a correction to these well-known results. For $d_N = 0$, we can evaluate both

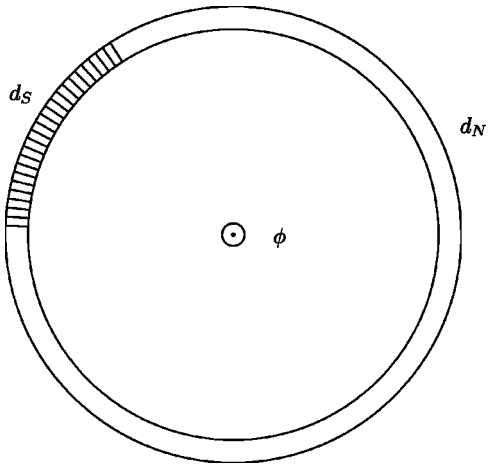

FIG. 1. NS ring composed of a normal segment N and a superconductor segment S, pierced by an Aharonov-Bohm flux ϕ.

terms and, by summation, reconstruct the short junction result: the current is $2\pi\Delta/\phi_o \sin(\Delta\chi/2)$ per channel.[6,7] As a result, we study the crossover from the persistent current to the Josephson current at finite temperature for single-channel and for multichannel NS loops.

The paper is organized as follows: in Sec. II, we recall the expression of the thermodynamic potential in terms of the excitation spectrum and we derive the excitation spectrum of a single-channel NS loop for arbitrary d_N and d_S. In Sec. III, we derive our new decomposition of the current and evaluate the contribution of the nonlinear flux dependent energy levels. In Sec. IV, we apply this approach to demonstrate the BK result valid in the case of a long normal segment and we consider the evolution of the full spectrum when d_S varies. Section V describes the crossover from long SNS junctions to short junctions as d_N is decreased. The contributions to the ground state current from levels above and below the gap Δ is discussed in Sec. VI. Finite temperature effects are incorporated in Sec. VII to study the transition from a diamagnetic to a paramagnetic behavior at small flux when d_S is lowered or when T is increased. Finally, in Sec. VIII we show how to sum over transverse channels to obtain the multichannel case from our study of the single-channel case. We conclude in Sec. IX.

II. EXCITATION SPECTRUM AND SUPERCURRENT OF THE NS LOOP

A. Relation between supercurrent and excitation spectrum

We consider a NS loop of perimeter L made of a superconducting segment of length d_S and a normal segment of length d_N. The nondissipative current flowing in this system is obtained by differentiation of the thermodynamic potential or Gibbs energy $\Omega(T,\mu,\phi)$ with respect to the magnetic flux:

$$I(\phi) = -\left(\frac{\partial\Omega}{\partial\phi}\right)_{\mu,T}. \tag{1}$$

For a system with inhomogeneous superconductivity, Bardeen *et al.* and Beenakker *et al.* have shown that it is possible to express the thermodynamic potential in terms of the excitation spectrum.[8,9] This excitation spectrum is found by solving the Bogoliubov–de Gennes equations:[10]

$$\begin{pmatrix} H_o & \Delta(x) \\ \Delta^*(x) & -H_o^* \end{pmatrix} \begin{pmatrix} u(x) \\ v(x) \end{pmatrix} = \epsilon \begin{pmatrix} u(x) \\ v(x) \end{pmatrix}. \tag{2}$$

These equations apply when the normal segment is shorter than the phase coherence length L_ϕ. For such a mesoscopic NS ring, excitations are coherent around the whole loop and can be described by electronlike and holelike wave functions denoted, respectively, by $u(x)$ and $v(x)$. $H_o = [-i\hbar d/dx - qA(x)]^2/2m + V(x) - \mu$, where μ is the chemical potential and m is the effective mass of electrons and holes common for both superconducting and normal parts. $A(x)$ is the vector potential due to the Aharonov-Bohm flux, $V(x)$ is the disorder potential, and x is the coordinate along the loop. In this paper, we consider the clean system $V(x)=0$. Following BK, we choose a ''square well'' model for the superconducting gap: $\Delta(x)$ is zero in the normal region and uniform $\Delta(x)=\Delta$ in the superconductor. The thermodynamic potential can be written in terms of the excitation energies and of the superconducting gap:

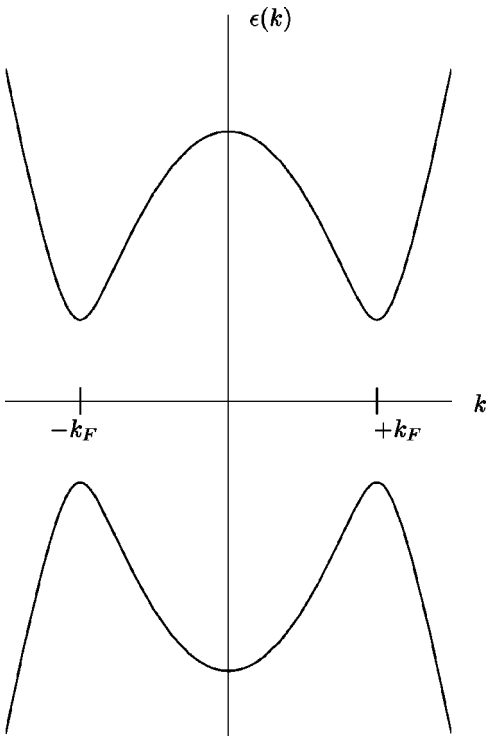

FIG. 2. Excitation spectrum (top curve) vs semiconductor model spectrum (top+bottom curves) of a large purely superconducting ring.

$$\Omega(T,\mu,\phi) = -2T\int_0^\infty d\epsilon \ln\left(2\cosh\frac{\epsilon}{2T}\right)\rho_{exc}(\epsilon,\phi) + g^{-1}\int dx|\Delta(x)|^2 + \mathrm{Tr}\,H_o, \tag{3}$$

where g is the pairing interaction present in the superconducting segment. In front of the first integral, the factor 2 accounts for spin degeneracy, and we choose units with $k_B=1$. In this formula, $\rho_{exc}(\epsilon,\phi)$ is the density of excited states per spin direction. The last two terms in Eq. (3) are independent of the flux. The first term can be interpreted as the Gibbs energy for the semiconductor model. In the semiconductor model, states with positive energies lie at the quasiparticle energies of the initial problem and states below the Fermi level lie at the opposite of the former quasiparticles energies, as depicted in Fig. 2. By construction, the spectrum of this semiconductor model is fully symmetric with respect to its Fermi level and each state can only be singly occupied. For this semiconductor, the flux dependent part of the thermodynamical potential is

$$\Omega(T,\mu,\phi) = -T\int_{-\infty}^{\infty} d\epsilon \ln\left(1+\exp-\frac{\epsilon}{T}\right)\rho(\epsilon,\phi), \tag{4}$$

where $\rho(\epsilon,\phi)=\rho_{exc}(|\epsilon|,\phi)$ is the semiconductor density of states obtained by symmetrization of the original density of excited states as represented in Fig. 2.

B. Excitation spectrum for arbitrary NS loop

1. Derivation of the spectrum

In this section, we calculate the flux-dependent excitation spectrum $\epsilon(\phi)$ of the NS loop. BK have established this excitation spectrum below the gap Δ for a fixed number N of electrons per spin direction.[1] Here, we calculate the spectrum below and above Δ, considering as well the cases of a fixed number of particles or a fixed chemical potential $\mu=k_F^2/2m$. The case of a fixed number of electrons per spin direction corresponds to $k_F L=\pi N$.[11] The excitation energies are found by solving the Bogoliubov–de Gennes equation (2) for the NS loop. The eigenvalue equation is obtained by matching the two-component wave functions and their derivatives at the NS interfaces; see Appendix A. In the quasiclassical approximation $\epsilon \ll E_F$, the resulting equation is

$$\cos k_F L = r_\epsilon \cos\left(\frac{\epsilon d_N}{\hbar v_F} \mp 2\pi\varphi + \Theta_\epsilon\right), \tag{5}$$

where $\varphi=\phi/\phi_o$ is the reduced flux. The minus sign corresponds to excitations around $+k_F$ and the plus sign to excitations around $-k_F$. Θ_ϵ is a phase shift due to the presence of the superconductor that adds to the phase shift associated to the motion in the normal segment. The function r_ϵ defines an energy dependent renormalization of the Fermi wave vector $\cos k_F L \to \cos k_F L/r_\epsilon$. The functions r_ϵ and Θ_ϵ have different expressions below and above the gap. Inside the gap $\epsilon<\Delta$, they are given by (see appendix A)

$$r_\epsilon e^{i\Theta_\epsilon}=\frac{\sinh(2i\eta_\epsilon-\lambda_\epsilon d_S)}{\sinh 2i\eta_\epsilon}, \tag{6}$$

where $e^{2i\eta_\epsilon}=(\epsilon+i\sqrt{\Delta^2-\epsilon^2})/\Delta$ and $\lambda_\epsilon=\sqrt{\Delta^2-\epsilon^2}/\hbar v_F$. At zero energy, $\lambda=\lambda_{\epsilon=0}$ is the inverse of the superconducting coherence length $\xi_o=\hbar v_F/\Delta$ which is the characteristic length scale for this system.[12] The modulus of the complex number (6) is

$$r_\epsilon=|\cosh\lambda_\epsilon d_S+i\cot 2\eta_\epsilon \sinh\lambda_\epsilon d_S|, \tag{7}$$

and the phase Θ_ϵ satisfies

$$\tan\Theta_\epsilon=\cot 2\eta_\epsilon \tanh\lambda_\epsilon d_S. \tag{8}$$

Above the gap, Eq. (6) becomes (see Appendix A)

$$r_\epsilon e^{i\Theta_\epsilon}=\frac{\sinh(i\delta k_\epsilon d_S+2\delta_\epsilon)}{\sinh 2\delta_\epsilon} \tag{9}$$

$$=\cos\delta k_\epsilon d_S+i\coth 2\delta \sin\delta k_\epsilon d_S, \tag{10}$$

so that Θ_ϵ and r_ϵ satisfy

$$r_\epsilon=|\cos\delta k_\epsilon d_S+i\coth 2\delta_\epsilon \sin\delta k_\epsilon d_S| \tag{11}$$

and

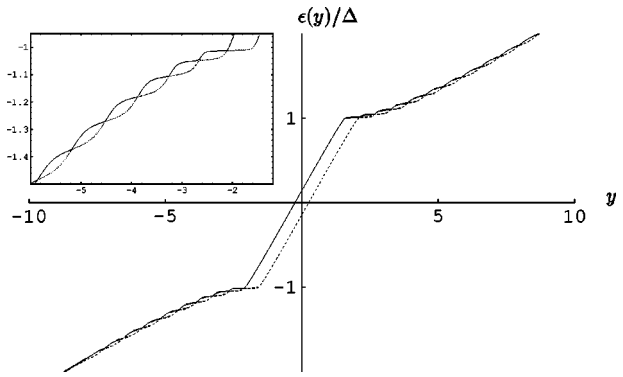

FIG. 3. $\epsilon^j(y)$ for $j=+1$ (solid line) and $j=-1$ (dashed line) in a NS loop with $d_S=20\xi_o$, $d_N=10\xi_o$, containing an even number of electrons per spin direction.

$$\tan\Theta_\epsilon=\coth 2\delta_\epsilon \tan\delta k_\epsilon d_S, \tag{12}$$

where $e^{2\delta_\epsilon}=(\epsilon+\sqrt{\epsilon^2-\Delta^2})/\Delta$ and $\delta k_\epsilon=\sqrt{\epsilon^2-\Delta^2}/\hbar v_F$. We choose Θ_ϵ to have the same integer part as $\delta k_\epsilon d_S$. This implies

$$\Theta_\epsilon=\arctan\left(\frac{\tan\delta k_\epsilon d_S}{\tanh 2\delta_\epsilon}\right)+\pi Int\left(\frac{\delta k_\epsilon d_S}{\pi}+\frac{1}{2}\right). \tag{13}$$

The spectrum above the gap $\epsilon>\Delta$ was not considered in the work of BK. Excitation energies are thus solutions of the quantization equation (5) valid whether the energy is above or below Δ. The complexity is hidden in the energy dependence of the functions r_ϵ and Θ_ϵ given respectively by Eqs. (7), (11), and Eqs. (8), (12), and (13). These functions are plotted in Figs. 13–15 of Appendix A. The correspondence between the solutions above and below the gap is given by the mapping:

$$-i\eta_\epsilon \to \delta_\epsilon$$

$$\lambda_\epsilon \to i\delta k_\epsilon. \tag{14}$$

The excitation energies are the positive solutions of Eq. (5). They are quantized according to $\epsilon^j(n\pm\varphi)$, the two functions $\epsilon^j(y)$ being

$$\epsilon^j(y)=\frac{h v_F}{d_N}\left[y-\frac{\Theta_\epsilon}{2\pi}+\frac{j}{2\pi}\arccos\left(\frac{\cos k_F L}{r_\epsilon}\right)\right], \tag{15}$$

where $j=\pm 1$. All the information about the spectrum and its flux dependence is contained in the functions $\epsilon^j(y)$. We use these functions to calculate the current in the following sections. As an example, in Fig. 3 we have plotted the two functions $\epsilon^j(y)$ for a NS loop with $d_S=20\xi_o$ and $d_N=10\xi_o$ containing an even number of particles per spin direction.

2. Linear and nonlinear regions of the NS loop spectrum

The flux dependent spectrum is obtained by folding the curves $\epsilon^j(y)$ in the interval $[-1/2,1/2]$. This is shown in Fig. 4 for the example $d_S=20\xi_o$ and $d_N=10\xi_o$. At zero flux, the first energy levels $\epsilon^j(n,\varphi=0)$ correspond to $(n,j)=(0,1),(1,-1),(1,1),(2,-1)$, etc. Now, we examine the

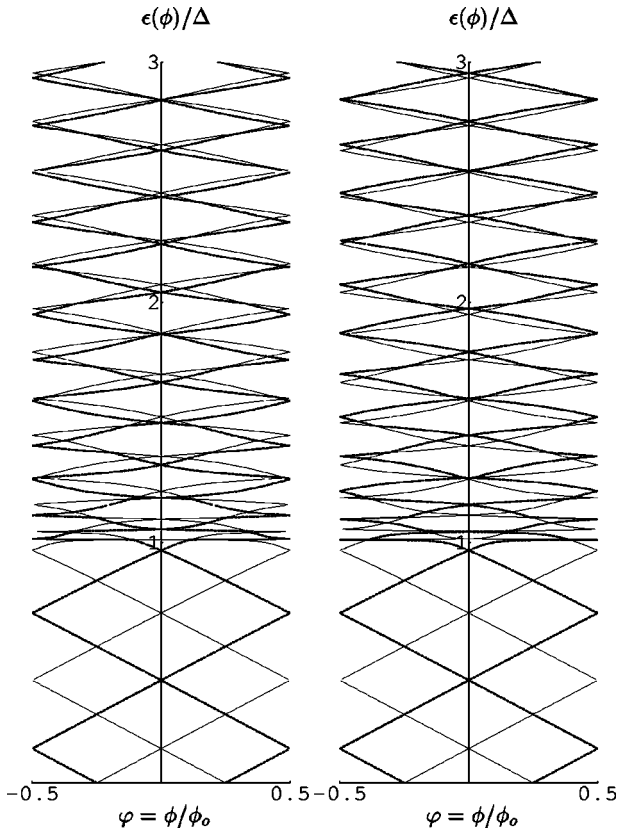

FIG. 4. NS loop spectrum $\epsilon^j_\pm(n,\varphi)$ for $j=+1$ (thin line) and $j=-1$ (thick line) $d_S=20\xi_o$, $d_N=10\xi_o$ for even (left) and odd (right) numbers of electrons N per spin direction. For large energies, the two branches $j=\pm1$ tend to coincide. The high energy levels exhibit a parity effect and are close to those of the normal ring. The Andreev levels are insensitive to the parity of N.

general structure of the excitation spectrum for arbitrary values of d_N or d_S. We distinguish three regions.

(i) The low energy spectrum $\epsilon<\Delta$: in this limit, $\Theta_\epsilon \simeq \epsilon/\Delta \times \tanh \lambda d_S$ and $r_\epsilon \simeq \cosh \lambda d_S$. The resulting form of the spectrum equation (5) is

$$\frac{\cos k_F L}{\cosh \lambda d_S} \simeq \cos\left(\frac{\epsilon d^*}{\hbar v_F} \mp 2\pi\varphi\right), \tag{16}$$

and the energy levels vary linearly with the magnetic flux,

$$\epsilon^j_\pm(n,\varphi) = \frac{h v_F}{d^*}\left[n \pm \varphi + \frac{j}{2\pi}\arccos\left(\frac{\cos k_F L}{\cosh \lambda d_S}\right)\right], \tag{17}$$

where $d^* = d_N + \xi_o \tanh \lambda d_S$ is the effective size of the normal segment. The low energy flux dependent spectrum is made of linear sections with slopes $\pm e v_F/d^*$. There are two sets of levels corresponding to $j=+1$ and $j=-1$. Each set is made of equally spaced levels with a common average spacing $h v_F/2d^*$. The energy shift between the two sets is $h v_F/\pi d^* \times \arccos(\cos k_F L/\cosh \lambda d_S)$. For $d_S \gg \xi_o$, this shift is $h v_F/2d^*$. Taking into account the spin degeneracy, there are $4d^*/\pi\xi_o$ quasiparticle states inside the gap.

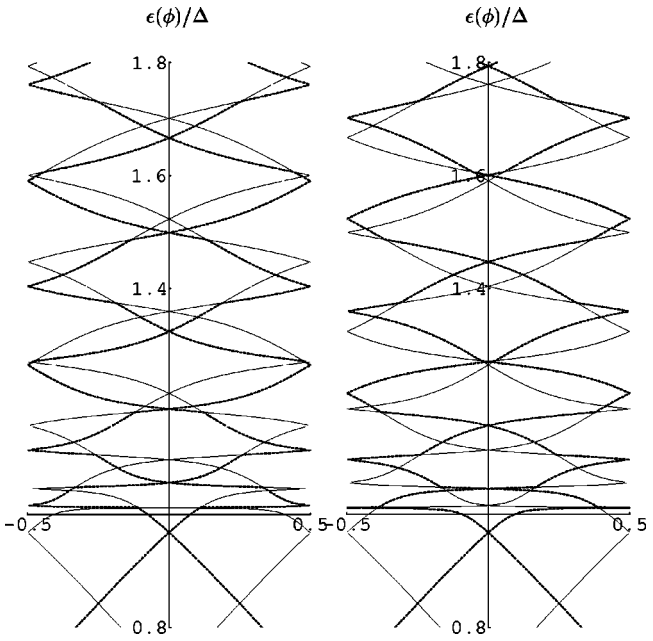

FIG. 5. NS loop spectrum $\epsilon^j_\pm(n,\varphi)$ in the vicinity of Δ for $j=+1$ (thin line) and $j=-1$ (thick line) $d_S=20\xi_o$, $d_N=10\xi_o$ and N even (left) or odd (right).

(ii) The high energy spectrum $\epsilon \gg \Delta$: then $\Theta_\epsilon \simeq \delta k_\epsilon d_S \simeq \epsilon d_S/\hbar v_F$ and $r_\epsilon \simeq 1$. Equation (5) takes the asymptotic form

$$\cos k_F L \simeq \cos\left(\frac{\epsilon L}{\hbar v_F} \mp 2\pi\varphi\right), \tag{18}$$

and the spectrum is linear in flux:

$$\epsilon^j_\pm(n,\varphi) = \frac{h v_F}{L}\left[n \pm \varphi + \frac{j}{2\pi}\arccos(\cos k_F L)\right]. \tag{19}$$

The high energy spectrum has the same linear structure as the low energy spectrum but with a smaller slope $\pm e v_F/L$ which corresponds to excitations extended around the whole loop. Indeed, Eq. (19) is the linearized excitation spectrum of a purely normal ring of perimeter $L=d_S+d_L$. For a given parity, $\cos k_F L=\pm1$, the two sets of levels $j=+1$ and $j=-1$ are in coincidence, as depicted in Fig. 4.

(iii) Between regions (i) and (ii), the curvature $\partial^2\epsilon/\partial^2\phi$ is finite and alternates in sign. It is impossible to linearize the spectrum in this region plotted in Fig. 5. One has to be very careful in evaluating the current carried by these levels. This will be done in Sec. III.

C. From the normal ring to the SNS junction

In the limit $d_S/\xi_o=0$, we have $\Theta_\epsilon=0$ and $r_\epsilon=1$ and we recover the quantization condition for a normal ring of length L:

$$\cos k_F L = \cos\left(\frac{\epsilon L}{\hbar v_F} \mp 2\pi\varphi\right). \tag{20}$$

The corresponding linearized spectrum is

$$\epsilon_{\pm}^{j}(n,\varphi)=\frac{hv_F}{L}\left[n\pm\varphi+\frac{j}{2\pi}\arccos(\cos k_F L)\right], \quad (21)$$

characteristic of a purely normal ring.[13] In Eq. (21), $\pm\varphi$ stands for excitations with momentum around $\pm k_F$. The index $j=1$ corresponds to holelike excitations with $|k|<k_F$ and $j=-1$ to electronlike excitations $|k|>k_F$.

In the opposite limit, for large d_S/ξ_o, $1/r_\epsilon$ is vanishingly small in the gap region and Θ_ϵ is simply related to the Andreev energy dependent phase shift at a NS interface by $\Theta_\epsilon=\pi/2-\arccos(\epsilon/\Delta)$. Consequently, the Andreev level spectrum given by Eq. (15) becomes

$$\epsilon_{\pm}^{j}(n,\varphi)=\frac{hv_F}{d_N}\left[n\pm\varphi+\frac{1}{2\pi}\arccos\frac{\epsilon}{\Delta}+\frac{j-1}{4}\right]. \quad (22)$$

We can express this latter spectrum with only one quantum number $m=2n+(j-1)/2$, the first excited states at zero flux corresponding to $m=0,1,2,$ etc.:

$$\epsilon_{\pm}(m,\varphi)=\frac{hv_F}{2d_N}\left[m\pm 2\varphi+\frac{1}{\pi}\arccos\frac{\epsilon}{\Delta}\right]. \quad (23)$$

We recognize in Eq. (23) the spectrum discovered by Kulik for bound states in a SNS junction,[14] the difference between the phases χ_1 and χ_2 of the superconducting order parameters of the leads being $\chi_1-\chi_2=4\pi\varphi=4\pi\phi/\phi_o$. This spectrum can be understood in terms of quantization along closed orbits in which one electron propagates in one direction along the normal segment, is reflected as a hole at the superconductor interface with a phase shift $\chi_{1S}-\arccos(\epsilon/\Delta)$; then the hole goes back along the normal segment and is finally reflected as an electron with an additional phase shift $-\chi_{2S}-\arccos(\epsilon/\Delta)$. This explains why the level spacing at $\chi_{1S}=\chi_{2S}$ is $hv_F/2d_N$ corresponding to a box of size $2d_N$. This scheme applies because the electron cannot tunnel through the superconductor in the regime $d_S\gg\xi_o$.

III. HARMONIC EXPANSION OF THE SUPERCURRENT

In Sec. II, we have shown that the NS spectrum can be linearized for low and high energies compared to Δ. Close to the gap edge, we have identified a complicated nonlinear variation of the levels with the flux. Instead of the usual decomposition between current carried by the Andreev levels and by the levels above the gap,[15,16] we demonstrate that one can extract a contribution to the current harmonics specifically due to the nonlinearities, namely, a term proportional to $\partial^2\epsilon/\partial^2\phi$. Here, the nonlinearities occur because a quasiparticule experiences an energy dependent phase shift when it goes through the NS boundary. Our approach is quite general and can be applied for other systems where a nonlinear behavior occurs. As an example, in Appendix C, we use this formalism to calculate the correction to persistent current of the normal ring with a quadratic dispersion relation.

A. Derivation of the main result

We start within the framework of the semiconductor model and we use the functions $\epsilon^j(\varphi)$ introduced in Sec. II. In order to simplify the notations, we first write the current for one value of j and omit the index j for convenience. Hence, we consider the spectrum $\epsilon(n\pm\varphi)$ and $n=\ldots,-1,0,1,\ldots$ in the semiconductor model representation. We can express the Gibbs energy [Eq. (4)] in terms of the double integral of the density of states $N(\epsilon,\phi)$ defined by

$$N(\epsilon,\phi)=\int_{-\infty}^{\epsilon}d\epsilon'\int_{-\infty}^{\epsilon'}d\epsilon''\rho(\epsilon'',\phi) \quad (24)$$

in the following manner:

$$\Omega(T,\mu,\phi)=\int_{-\infty}^{\infty}d\epsilon N(\epsilon,\phi)\left(\frac{\partial f}{\partial\epsilon}\right), \quad (25)$$

leading to the current given by Eq. (1):

$$I(\phi)=\int_{-\infty}^{\infty}\frac{d\epsilon}{4T\cosh^2\epsilon/2T}\left(\frac{\partial N(\epsilon,\phi)}{\partial\phi}\right)_{\mu}. \quad (26)$$

The quantities $\rho(\epsilon,\phi)$ and $N(\epsilon,\phi)$ are even functions of the magnetic flux. Omitting the flux independent part, we write the Fourier decomposition of $N(\epsilon,\phi)$ as

$$N(\epsilon,\phi)=\sum_{m=1}^{\infty}N_m(\epsilon)\cos 2\pi m\varphi. \quad (27)$$

The density of states of the semiconductor model is given by

$$\rho(\epsilon,\phi)=\sum_{n=-\infty,\sigma=\pm1}^{n=\infty}\delta[\epsilon-\epsilon(n+\sigma\varphi)]. \quad (28)$$

Using the Poisson summation formula, one gets the Fourier harmonics of the density of states,

$$\rho_m(\epsilon)=4\int_{-\infty}^{\infty}dy\cos 2\pi m y\,\delta[\epsilon-\epsilon(y)], \quad (29)$$

in terms of $\epsilon(y)$, which is given by Eq. (15) in the NS loop problem. After a double integration, one obtains the coefficients $N_m(\epsilon)$:

$$N_m(\epsilon)=4\int_{-\infty}^{y(\epsilon)}dy'\frac{\sin 2\pi m y'}{2\pi m}\frac{d\epsilon(y')}{dy'}. \quad (30)$$

Finally, the current is given by

$$I(\phi)=\sum_{m=1}^{\infty}I_m\sin 2\pi m\varphi, \quad (31)$$

with

$$I_m(T)=-\frac{2\pi m}{\phi_o}\int_{-\infty}^{\infty}\frac{d\epsilon}{4T\cosh^2\epsilon/2T}N_m(\epsilon). \quad (32)$$

At $T=0$, the current harmonics are given by $I_m(T=0) = -2\pi m N_m(\epsilon=0)/\phi_o$. Integrating Eq. (30) by parts, one gets

$$I_m(T=0) = \frac{2}{\pi m}\frac{1}{\phi_o}\left[\frac{d\epsilon}{dy}(y_o)\cos 2\pi m y_o - \int_{-\infty}^{y_o} dy \frac{d^2\epsilon}{d^2 y}\cos 2\pi m y\right], \quad (33)$$

with $y_o = y(\epsilon=0)$. We have assumed that the slope $d\epsilon/dy$ is vanishing at the bottom $y=-\infty$ of the semiconductor valence band. Equation (33) is the general expression of the current for a spectrum $\epsilon(n\pm\varphi)$. For the NS loop case, we have to sum contributions from the two branches of levels $j=\pm 1$. To understand Eq. (33), we recall that y plays the role of the reduced flux $\varphi=\phi/\phi_o$. The first term is related to the slope of $\epsilon(y)$ at zero energy, i.e., to the current $-\partial\epsilon/\partial\phi$ carried by the zero energy Andreev level. It leads to a triangular $I(\phi)$ current-flux relationship. The second term is a sum over the whole spectrum of an integrand proportional to $d\epsilon/dy$, i.e., $\partial^2\epsilon/\partial^2\phi$. Only the region around the gap edge with nonlinearities gives a non zero contribution, regardless whether these nonlinearities are located below or above Δ. For this reason, our representation of the current is different from the usual decomposition of the Josephson current for SNS junctions as a contribution from the discrete spectrum below the gap plus a contribution from the continuum spectrum above the gap.[15]

B. Numerical evaluation

In this section, we show that the relative weight of the two terms in Eq. (33) is related to the value of d_N. We evaluate numerically the integral term in Eq. (33) for loops with finite lengths $0\leqslant d_N\leqslant 10\xi_o$ and $0\leqslant d_S\leqslant 10\xi_o$. In Fig. 6, we have plotted the first $I_{m=1}$ and second $I_{m=2}$ harmonics of $I(\phi)$ as a function of d_N, for different values of d_S. The dashed lines represent the first term in Eq. (33) which corresponds to the Bardeen-Johnson (BJ) approximation used by BK. One sees that the second term is already negligible for $d_N\gtrsim 2$. For small values of d_N, both terms in Eq. (33) are of the same order of magnitude. The difference between the exact result and the BJ approximation, which is shown in the inset of Fig. 6 for $I_{m=2}$, decreases monotonically with increasing d_N. We note that this correction to the BJ approximation is roughly independent of d_S for $m=2$. As expected for odd harmonics, $I_{m=1}$ decreases as d_S increases; see Fig. 6. For $d_S=10\xi_o$, our numerical evaluation of the second harmonic is in good agreement with the analytical value $I_{m=2} = -16\Delta/3\phi_o$ expected for $d_N=0$ and $d_S=\infty$ from Eq. (B3).

C. Conclusion

We have identified a term specifically due to nonlinerities in the spectrum and we have shown numerically that it is small if $d_N\lesssim 2\xi_o$. In the following sections, we use Eq. (33) to recover analytical expressions in the extreme cases $d_N \gg \xi_o$ for any d_S (Sec. IV) and $d_S\gg\xi_o$ for $d_N\to 0$ (Sec. V).

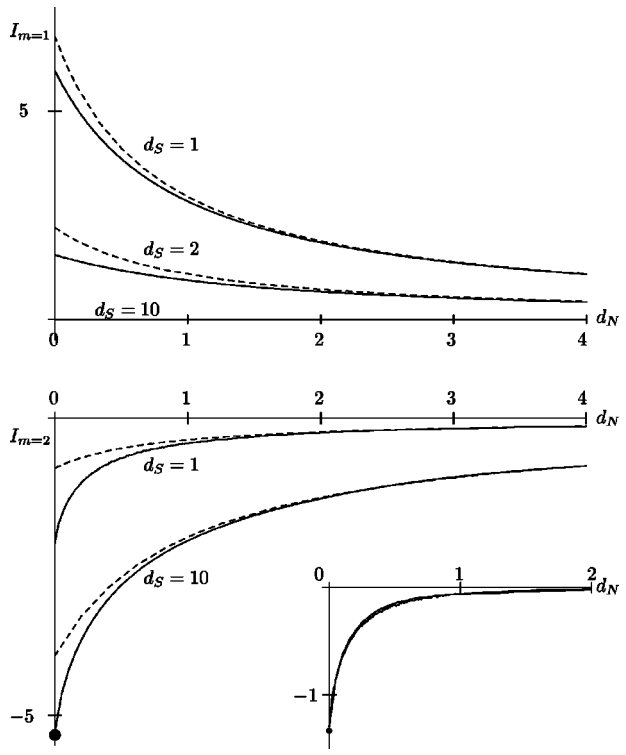

FIG. 6. First harmonic $I_{m=1}$ (top curve) and second harmonic $I_{m=2}$ (bottom curve) in units of Δ/ϕ_o as a function of d_N, for different values of d_S. Dashed lines represent the BJ approximation. The inset shows the difference between the second harmonic and its BJ evaluation for $d_S=1$ and 10. The dot represents the expected value for $d_N=0$ and $d_S\gg\xi_o$.

The decomposition [Eq. (33)] is valid for arbitrary d_N with $\epsilon^j(y)$ given by Eq. (15), and can be used to calculate the current-flux relationship in any NS loop. At a finite temperature, we find a crossover from paramagnetic to diamagnetic behavior at small flux when d_S is increased or T lowered; see Sec. VII.

IV. LONG NORMAL SEGMENT

In this section, we study the evolution of the spectrum and of $I(\phi)$ as a function of d_S for a NS ring with $d_N\gtrsim 2\xi_o$. We have shown in Sec. III B that in this case the second term in Eq. (33) is negligible.

A. Excitation spectrum for arbitrary d_S

In Figs. 7(a)–7(d), we have plotted the excitation spectrum for $d_S=0,\xi_o,5\xi_o,20\xi_o$ keeping d_N equal to $10\xi_o$. For the low energy part of these spectra, the flux dependence is linear with the slope $\pm hv_F/d_N$. For the normal ring $d_S=0$, the branches $j=\pm 1$ coincide, and we recover the spectrum of the normal ring with the double degeneracy due to the spin. For finite d_S, these branches are shifted by $\Delta\varphi = \pm\arccos[\cos(k_F L)/\cosh\lambda d_S]/2\pi$. For $d_S=5\xi_o$ and $d_S=20\xi_o$, they are shifted by half a quantum of flux $\phi_o/2$. Indeed, the low energy excitation spectrum is the same as the spectrum of a normal ring of perimeter d^* and with $\cos k_F L$ replaced by $\cos k_F L/\cosh\lambda d_S$. The low energy spectra for

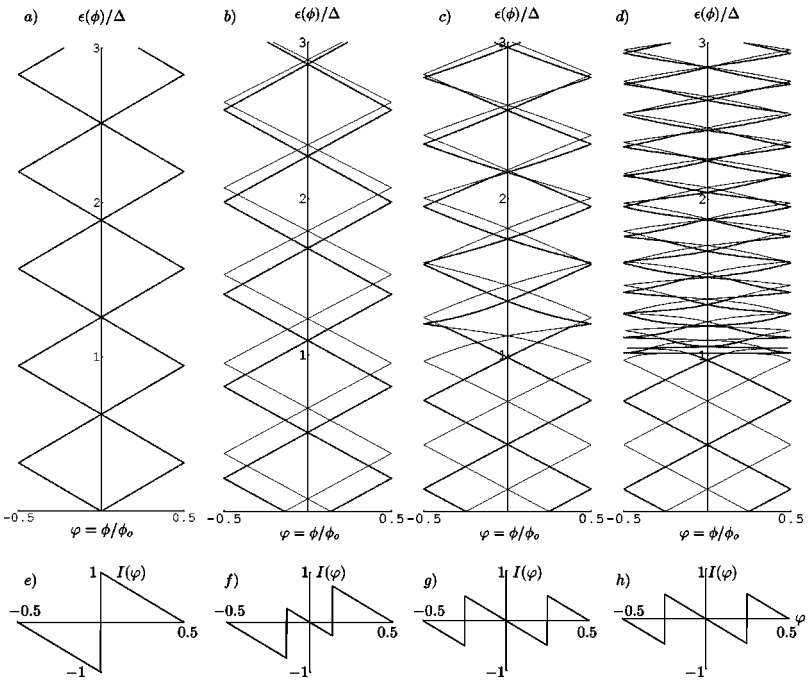

FIG. 7. NS loop spectrum $\epsilon^j_{\pm}(n,\varphi)$ for (a) $d_S=0$, (b) $d_S=\xi_o$, (c) $d_S=5\xi_o$, and (d) $d_S=20\xi_o$, keeping d_N equal to $10\xi_o$. The number of electrons per spin direction N is even. Levels with $j=+1$ correspond to the thin lines and those with $j=-1$ to the thick lines. The currents (e), (f), (g), and (h) are plotted in units of $I_o=2ev_F/d^*$ below the corresponding specta (a), (b), (c), and (d).

$d_S=5\xi_o,20\xi_o$, and ∞ are quite similar and correspond to quasiparticle motion confined in the normal region of the loop. The spectrum above the gap is more sensitive to the value of d_S because the level spacing scales as $1/L$ corresponding to a quasiparticle motion confined in the whole loop of length $L=d_S+d_N$.

B. Current-flux relationship for arbitrary d_S

The Fourier coefficients in the harmonics expansion of the current [Eq. (31)] are $I_m=I_m^+ + I_m^-$, with

$$I_m^j=\frac{2}{\pi m}\frac{1}{\phi_o}\frac{d\epsilon^j}{dy}(y_o^j)\cos 2\pi m y_o^j, \tag{34}$$

and they depend only on the zero energy Andreev level. Equation (15) yields

$$2\pi y_o^j=-j\arccos\left(\frac{\cos k_F L}{\cosh\lambda d_S}\right), \tag{35}$$

and $d\epsilon^j/dy=hv_F/d^*=E_A$. The energy E_A is the typical displacement of one energy level when the flux is varied. This is also the energy spacing between Andreev levels. The order of magnitude of the critical current is then E_A/ϕ_o. According to Eq. (33), the Fourier expansion of the current for arbitrary d_S reads

$$I(\phi)=\frac{4}{\pi}\frac{ev_F}{d^*}\sum_{m=1}^{\infty}\frac{T_m(X)}{m}\sin 2\pi m\phi/\phi_o, \tag{36}$$

with

$$X=\frac{\cos k_F L}{\cosh\lambda d_S} \tag{37}$$

and

$$T_m(X)=\cos(m\arccos X). \tag{38}$$

The coefficients $T_m(X)$ are the mth order Tchebytchev polynomials. The parameter X depends both on the band filling and on the crossover parameter λd_S. The first Tchebychev polynomials are $T_1(X)=X$, $T_2(X)=2X^2-1$, $T_3(X)=4X^3-3X,\ldots$. For a fixed number of electrons per spin direction, namely, for $\cos k_F L=\pm 1$, the beginning of the current expansion is given by the following expression:[17]

$$I(\phi)=\frac{4}{\pi}\frac{ev_F}{d^*}\left[\pm\frac{1}{\cosh\lambda d_S}\sin 2\pi m\phi/\phi_o + \frac{1-\sinh^2\lambda d_S}{2\cosh^2\lambda d_S}\sin 4\pi m\phi/\phi_o+\cdots\right]. \tag{39}$$

The formula above describes the suppression of the first harmonic $m=1$ when d_S goes to infinity. The suppression of odd harmonics is a general feature of the crossover from persistent current in normal loops to Josephson current in SNS junctions.

C. Case $d_S \gg \xi_o$: Josephson limit

We recall that for large d_S, the NS loop threaded by a magnetic flux ϕ behaves like a SNS junction with a superconducting phase shift $4\pi\phi/\phi_o$ between the leads. In this $d_S\to\infty$ limit, the functions $\epsilon^j(y)$ are flat outside the gap. Due to the infinite size of the system, the spectrum becomes a true continuum above the gap. Far from the gap, the density of levels is given by

$$\frac{dy}{d\epsilon}=\frac{d_N}{hv_F}+\frac{d_S}{hv_F}\frac{\epsilon}{(\epsilon^2-\Delta^2)^{1/2}}. \tag{40}$$

It is obtained from expressions (11), (13), and (15). The first term is the density of levels in a normal ring of perimeter d_N at the Fermi level and the second term is the BCS singularity at Δ. At $\epsilon \gg \Delta$, the total density of levels tends to those of a normal loop of perimeter $L = d_S + d_N$. Inside the gap for $\epsilon < \Delta$, we have

$$2\pi y^j(\epsilon) = \frac{\epsilon d_N}{\hbar v_F} - \arccos\frac{\epsilon}{\Delta} + (1-j)\frac{\pi}{2}, \tag{41}$$

which corresponds to the Kulik spectrum [Eq. (22)]. It is dominated by the linear behavior of the first term for long junctions $d_N \gg \xi_o$, except very close to Δ. Below the gap, the flux dependent spectrum is similar to those plotted in Figs. 7(c) and 7(d). In this limit, $X \to 0$ and only even $m = 2p$ harmonics are non zero in Eq. (36) because $T_{2p+1}(0) = 0$. This leads to the following $\phi_o/2$ periodic current:

$$I(\phi) = \frac{2}{\pi}\frac{ev_F}{d_N + \xi_o}\sum_{p=1}^{\infty}\frac{(-1)^p}{p}\sin 4\pi p\,\phi/\phi_o. \tag{42}$$

This is the Fourier expansion of a sawtooth current-flux relationship for the purely longitudinal channel of long SNS junctions. In Sec. VIII, we show that it corresponds to the result of Bardeen and Johnson.[3]

D. Case $d_S = 0$: persistent currents in normal rings

If we remove the superconductor, the parameter X is equal to $\cos k_F L$ and the effective length d^* is the perimeter L. Then, the model describes the persistent current in a purely normal ring of length L with fixed chemical potential. We recover the well-known result[18]

$$I(\phi) = \frac{4}{\pi}\frac{ev_F}{L}\sum_{m=1}^{\infty}\frac{\cos mk_F L}{m}\sin 2\pi m\,\phi/\phi_o; \tag{43}$$

the current $I(\phi)$ includes both spin directions. This result is correct in the framework of the quasi-classical approximation $\epsilon \ll E_F$. In fact, Eq. (43) is the zero order contribution in the $1/k_F L$ expansion. The following term in this expansion is due to the quadratic dispersion relation of free electrons and is evaluated in Appendix C.

V. LONG SUPERCONDUCTING SEGMENT

We consider now the case of large d_S and we study the crossover from long to short SNS junctions obtained by decreasing d_N. For vanishing d_N, the levels acquire a nonlinear behavior over a large energy range of order Δ. Then, the two terms in the decomposition Eq. (33) become of the same order of magnitude. For $d_N = 0$, we analytically recover the current through a short SNS junction.

A. Excitation spectrum for arbitrary d_N

In Figs. 8(a)–8(c), we have plotted the excitation spectrum for $d_N = 0, \xi_o$, and $10\xi_o$ and for $d_S = 20\xi_o$. For $d_N = 0$, there is only one spin degenerate Andreev level in the gap. As d_N is increased, new Andreev levels appear; see Figs. 8(a)–8(c). As discussed in Sec. II B, the number of

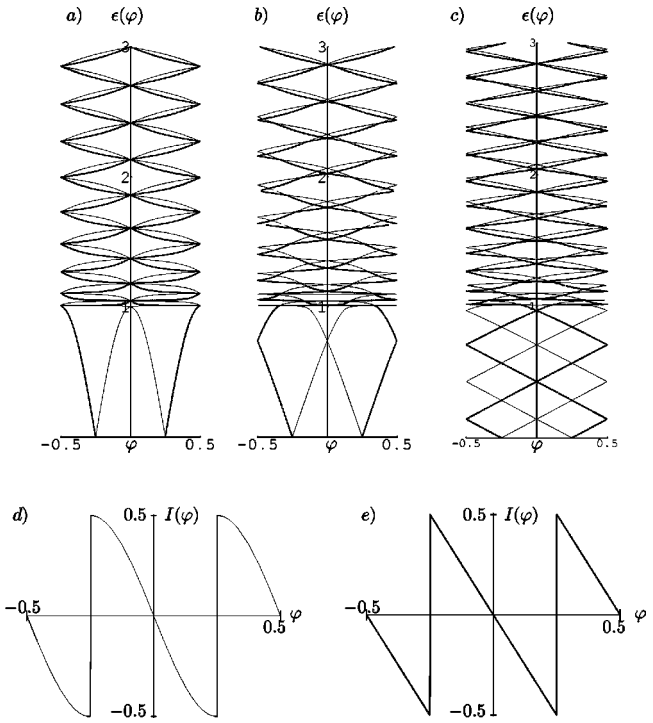

FIG. 8. NS loop spectrum $\epsilon^j_{\pm}(n,\varphi)$ for $d_S = 20\xi_o$ and (a) $d_N = 0$, (b) $d_N = \xi_o$, and (c) $d_N = 10\xi_o$. The currents (d) and (e) are expressed in units of $I_o = 2ev_F/d^*$, and correspond, respectively, to spectra (a) and (c). Levels with $j = +1$ correspond to the thin lines and those with $j = -1$ to the thick lines.

Andreev levels is roughly $4(d_N/\xi_o + 1)/\pi$. The spectrum is linear at low energy and only the last Andreev level at the vicinity of Δ varies nonlinearly with the magnetic flux.

B. Current-flux relationship for $d_N = 0$: short junctions

In the short junction limit $d_N = 0$, the eigenvalue equation is

$$2\pi y^j(\epsilon) = -\arccos\frac{\epsilon}{\Delta} + (1-j)\frac{\pi}{2}. \tag{44}$$

The function $\epsilon^j(y)$ is plotted in Appendix B. There is only one Andreev level in the gap which corresponds alternalively to $j = 1$ or $j = -1$. The spectrum can be written as

$$\epsilon(\phi) = \Delta\left|\cos 2\pi\phi/\phi_o\right|. \tag{45}$$

At $T = 0$, the current corresponding to this unique Andreev level is $\phi_o/2$ periodic and given by

$$I(\phi) = -2\pi\frac{\Delta}{\phi_o}\sin 2\pi\phi/\phi_o \tag{46}$$

for $|\phi/\phi_o| < 1/4$; see Fig. 8(d). This result was obtained by Kulik-Omel'yanchuk[6] and Beenakker and van Houten.[7] In Appendix B, we show how to recover this result from our formalism and Eq. (33). In this case, both terms in this equation contribute with the same order of magnitude, so that the BJ approximation clearly breaks down for $d_N = 0$.

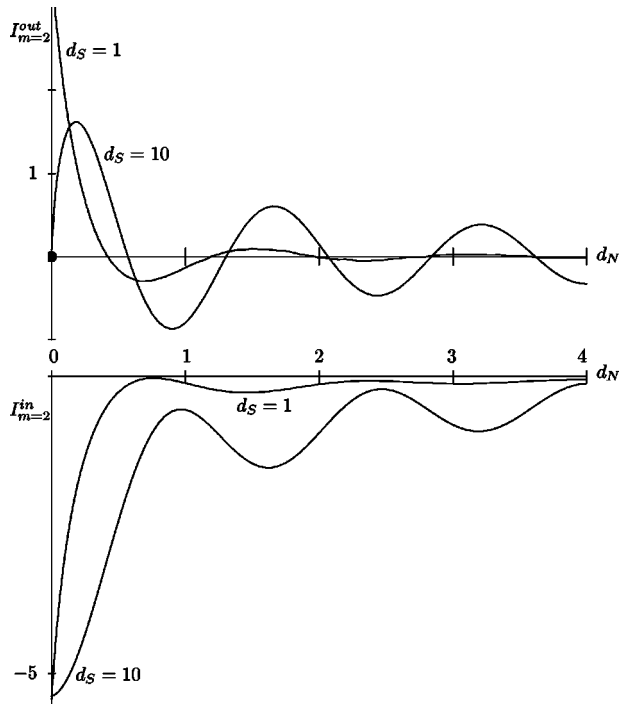

FIG. 9. Contributions to the second harmonic from states outside the gap $I^{out}_{m=2}$ and from states below the gap $I^{in}_{m=2}$ in units of Δ/ϕ_o for $d_S=\xi_o$ and $d_S=10\xi_o$ as a function of d_N. The dot represents the expected cancellation of the current carried by states above the gap in the limit of large d_S.

Finally, we can compare the short d_N case, $\Delta<E_A=hv_F/d^*$, and the long d_N case, $\Delta>E_A$, developed in Sec. IV. In both cases, the current is $\phi_o/2$ periodic, diamagnetic at small flux and there is a jump at $\phi_o/4$. In the former case, $I(\phi)$ is triangular and the critical current is of order E_A/ϕ_o. In the latter case, $I(\phi)$ has a sine dependence and the critical current is of order Δ/ϕ_o. It is a particular case of the well-known statement that the critical Josephson current in a SNS junction is given by the minimum of the two energy scales E_A and Δ,[19] E_A being the Thouless energy of the clean NS loop.

VI. WHICH LEVELS CARRY THE CURRENT?

The equilibrium current in a NS loop is carried both by levels below and above the superconducting gap Δ.[15,16] Although our formalism is based on a decomposition between linear vs nonlinear flux dependence of the levels, we can separate in each term of Eq. (33) into contributions from states above and below the gap. The result is shown in Fig. 9. Although the total current decreases monotonously with d_N, both contributions are oscillating functions of d_N. These oscillations in the subgap current harmonics correspond to the apparition of new Andreev levels below the gap when d_N increases. Since the number of Andreev levels is $4d^*/\pi\xi_0$, the oscillations have a periodicity $\pi\xi_0/2$. Although we have not checked this numerically, we believe that the contribution carried by the states outside the gap cancels whenever the level crossing the gap has zero slope. Otherwise, when an Andreev level crosses the gap, it still carries current on the other side of the gap.[15,17]

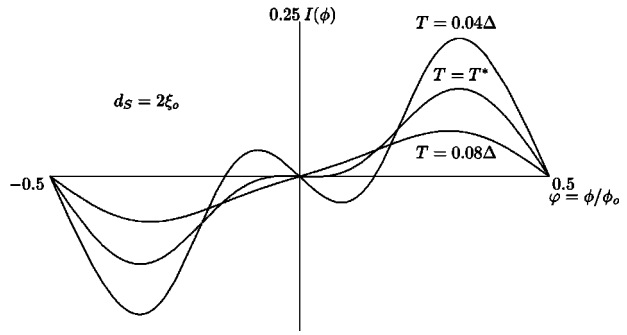

FIG. 10. Current-flux relationships for $d_S=2\xi_o$, $d_N=10\xi_o$ and for $\cos k_F L=1$. At $T=T^*=0.056\Delta$, the slope $\partial I/\partial\phi$ at the origin $\phi=0$ changes in sign. The current is represented in units of $I_o=\Delta/\phi_o$.

For the case of the short SNS junction, $d_N=0$ and $d_S\gg\xi_o$, the current is solely carried by the single Andreev level. As seen in Fig. 9, when d_S is close to ξ_o, there is a contribution from states above the gap, which is significant when d_S is close to ξ_o.

VII. TEMPERATURE EFFECT

We treat the effect of a finite temperature on the crossover from SNS junctions to normal rings. We essentially focus on the case $d_N\gtrsim 2\xi_0$.

A. Harmonics expansion at finite temperature

We use Eq. (32) to compute the harmonics of the current at finite temperature. Compared to Eq. (36), these harmonics are reduced by the following thermal factor:

$$I_m(T)=I_m(T=0)\frac{x}{\sinh x}, \tag{47}$$

with $x=2\pi^2 mT/E_A$. The characteristic energy scale associated with the m-th harmonic is given by E_A/m. The resulting current for $d_N\gtrsim 2\xi_o$ is

$$I(\phi,T)=8\pi\frac{T}{\phi_o}\sum_{m=1}^{\infty}\frac{T_m(X)}{\sinh\pi m\dfrac{T}{\Delta}\dfrac{d^*}{\xi_o}}\sin 2\pi m\phi/\phi_o, \tag{48}$$

where X and $T_m(X)$ are given by Eqs. (37) and (38).

B. Transition from dia- to paramagnetic loops

For N even, a normal ring has a paramagnetic magnetization at zero flux while a SNS junction carries a diamagnetic current. At $T=0$, the transition from diamagnetic to paramagnetic behavior occurs at $d_S=0$. At finite temperature, this transition occurs at a finite d_S. At fixed d_S and d_N, there is a similar crossover as a function of the temperature. In Fig. 10, we see that the slope at the origin of the $I(\phi)$ curve changes sign at $T=T^*(d_S,d_N)$. The small flux current is

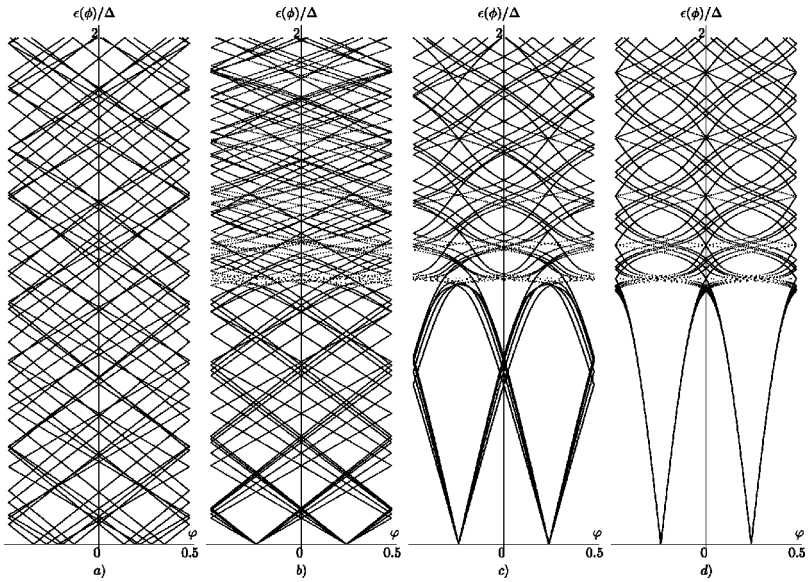

FIG. 11. Multichannel spectra. The cross section is a square of size $(2\lambda_F)^2$. For clarity, we have represented only a few flux-dependent channels among the $M=k_F^2 S/4\pi$ transverse channels. (a) $d_S=\xi_o$ and $d_N=10\xi_o$, (b) $d_S=10\xi_o$ and $d_N=10\xi_o$, (c) $d_S=10\xi_o$ and $d_N=\xi_o$, and (d) $d_S=10\xi_o$ and $d_N=0$.

diamagnetic for $T<T^*$ and paramagnetic for $T>T^*$. The function $T^*(d_S,d_N)$ is an increasing function of d_S and a decreasing function of d_N given by

$$T^*=\frac{\Delta d_S}{\pi d^*}. \tag{49}$$

This behavior can be understood from the harmonics expansion [Eq. (48)]. For N even, the first harmonic is paramagnetic while the second is diamagnetic. When the temperature is increased, the reduction of the second harmonic is stronger than for the first one and the resulting current becomes paramagnetic. The $I(\phi)$ curve for N odd is obtained by a $\phi_o/2$ translation of the $I(\phi)$ shown in Fig. 10. One sees that the magnetization at small flux is always diamagnetic. Indeed, all the harmonics are negative for N odd.

C. Ensemble average

Here, we calculate the average current of a large assembly of isolated single-channel NS loops with $d_N \gg \xi_o$ and a fixed number of particles. Statistically, half of them have an even number of electrons per spin direction N and for the others N is odd. As we have seen in Sec. VI, a transition from diamagnetism to paramagnetism occurs for the rings with even N, while the rings with N odd are always diamagnetic. Does the total orbital magnetism of the assembly exhibits a transition? We know that an assembly of normal rings has paramagnetic magnetization at small flux and is $\phi_o/2$ periodic.[20] In the opposite limit $d_S/\xi_o \gg 1$, the current in each loop is diamagnetic and $\phi_o/2$ periodic. The transition occurs at a very small value of d_S close to $0.5\xi_o$. In conclusion, we find that the current is always diamagnetic for values of d_S and d_N above ξ_o.

VIII. MULTICHANNEL RINGS

Up to now, we have considered a single-channel NS ring. From now on, we extend our study to multichannel NS rings. First, we present spectra with a small number of transverse channels and follow the evolution of the different channels when d_N and d_S are varied. Second, we study the crossover from Josephson current to persistent current in the clean multichannel NS loop at finite temperature.

The spectrum of clean multichannel rings can be obtained straightforwardly since the different channels are decoupled and characterized by their momenta k_y, k_z quantized along transverse directions y and z. The spectrum of each of these channels is simply obtained by the substitutions $v_F \to v_{Fx}$ and $k_F \to k_{Fx}$ in Eqs. (5) and (15). As an example, we have represented in Fig. 11 the spectra of a ring with a square section of size $(2\lambda_F)^2$ for different values of d_N and d_S. As $d_N \to 0$, the spectra of the different channels all shrink towards the single-channel spectrum and become completely degenerate when $d_N=0$. As a consequence, the $I(\phi)$ for a M-channel short junctions $d_N=0$ is exactly M times the single-channel result [Eq. (46)]. In long SNS junctions, the current $I(\phi)$ carried by any transverse channel has the same flux dependence as the longitudinal one, namely a triangular $I(\phi)$ with current jumps at $\phi=\pm\phi_o/4$. Nevertheless, the critical current is different for each channel as we can see from the spectra of Fig. 11, because the slopes $-\partial\epsilon/\partial\phi(\epsilon=0)$ are different. Finally, the total current stays proportional to the number of transverse channels M.

The total current is the sum of the single-channel currents. For $d_N \gtrsim 2\xi_o$, it is given by

$$I(\phi)=\frac{4}{\pi}\sum_{k_y,k_z}\frac{e v_{Fx}}{d_N+\xi_o}\sum_{m=1}^{\infty}\frac{T_m(X)}{m}\sin 2\pi m\varphi, \tag{50}$$

where

$$X=\frac{\cos k_{Fx}L}{\cosh \lambda d_S}. \tag{51}$$

In the case of a NS ring with many transverse channels, the discrete sum Eq. (50) over transverse channels can be replaced by an integral. Each channel carries a current given by Eq. (48) with $v_F \to v_{Fx}=v_F\cos\theta$, where θ is the angle

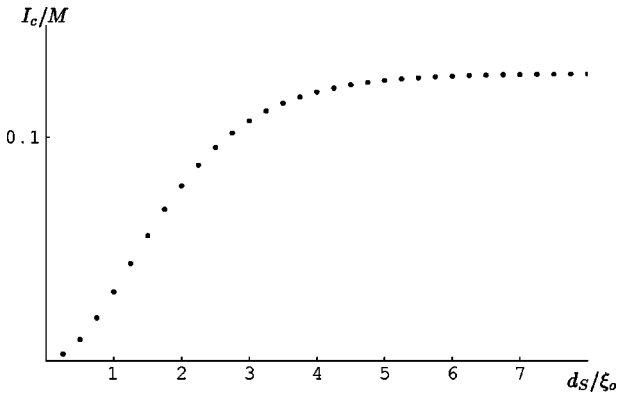

FIG. 12. Critical current per transverse channel as a function of d_S for $d_N=10$ and $k_F\xi_o \gg 1$ at $T=0.03\Delta$.

between the direction x and the Fermi momentum of the channel. By counting of the (k_y,k_z) satisfying $k_x^2+k_y^2+k_z^2=k_F^2$ for a given incidence θ, we obtain the total current

$$I(\phi)=16\pi M\frac{T}{\phi_o}\int_o^{\pi/2}d\theta\cos^2\theta \times\sum_{m=1}^{\infty}\frac{T_m(X)}{\sinh\pi m\frac{T}{\Delta}\frac{d^*}{\xi_o}}\sin 2\pi m\varphi, \tag{52}$$

where $M=k_F^2S/4\pi$ is the number of transverse channels. In the limit $d_S\gg\xi_o$ and at $T=0$, Eq. (52) leads to

$$I(\phi)=\frac{4M}{3\pi}\frac{ev_F}{d_N+\xi_o}\sum_{p=1}^{\infty}\frac{(-1)^p}{p}\sin 4\pi p\varphi. \tag{53}$$

The corresponding critical current is proportional to M:

$$I_c=\frac{2M}{3}\frac{ev_F}{d_N+\xi_o}. \tag{54}$$

This is the old result found by Bardeen and Johnson.[3] Ishii[4] and Svidsinski *et al.*[5] found different numerical prefactors.

In the opposite limit of the multichannel normal ring $d_S=0$, the total current averages to zero[21] for large $k_F\xi_o$. In Fig. 12, we show the the crossover of the critical current from $Mev_F/(d_N+\xi_o)$ for large d_S to zero as d_S approaches zero. This can be understood from the spectra of Fig. 11. Indeed, when d_S is large, the low energy spectra of each channel are in phase with $\epsilon=0$ for $\phi=\pm\phi_o/4$. When $d_S\to 0$, there is finite dephasing between the different spectra given by $\Delta\varphi=1/2\pi.\arccos X$ which leads to a cancellation of the total current.

IX. CONCLUSION

We have calculated the full excitation spectrum of a NS loop threaded by an Aharonov-Bohm flux, for any value of d_N and d_S: in particular, we have shown the spectrum of the NS loop above the gap. We have identified the contribution to the current directly originating from the nonlinearities in the flux dependent spectrum. We have recovered known results for short and long SNS junctions when $d_S\gg\xi_o$. For the single-channel NS ring at zero temperature, we have recovered the result of BK and our method allows us to clarify and justify the approximation made by BK. Moreover, we have extended the study of the NS loop to the finite temperature and to the multichannel cases.

ACKNOWLEDGMENTS

We would like to thank M. Büttiker, H. Bouchiat, and S. Gueron for useful and stimulating discussions.

APPENDIX A: NS LOOP EXCITATION SPECTRUM

We consider a purely one-dimensionnal NS loop with a superconducting segment in the region $0<x<d_S$ and a normal segment in $d_S<x<L$. This loop is threaded by a magnetic Aharonov-Bohm flux ϕ.

We first investigate states with energies below Δ. In the normal metal, the quasiparticles wavefunctions are plane waves oscillating at wavevectors $k_{e/h}=k_F\pm\epsilon/\hbar v_F$ just below (hole solution) or just above (electron solution) the Fermi momentum $+k_F$:

$$\begin{pmatrix}u(x)\\v(x)\end{pmatrix}=A\begin{pmatrix}1\\0\end{pmatrix}e^{ik_ex}+B\begin{pmatrix}0\\1\end{pmatrix}e^{ik_hx}. \tag{A1}$$

In the superconductor, they are

$$\begin{pmatrix}u(x)\\v(x)\end{pmatrix}=C\begin{pmatrix}e^{i\eta_\epsilon}\\e^{-i\eta_\epsilon}\end{pmatrix}e^{(ik_F-\lambda_\epsilon)x}+D\begin{pmatrix}e^{-i\eta_\epsilon}\\e^{i\eta_\epsilon}\end{pmatrix}e^{(ik_F+\lambda_\epsilon)x}, \tag{A2}$$

where $e^{2i\eta_\epsilon}=(\epsilon+i\sqrt{\Delta^2-\epsilon^2})/\Delta$ and $\lambda_\epsilon=\sqrt{\Delta^2-\epsilon^2}/\hbar v_F$. We express the continuity of these functions at the NS interfaces. In the presence of a reduced flux $\varphi=\phi/\phi_o$ it leads to the system

$$\begin{aligned}Ae^{ik_eL}&=e^{2\pi i\varphi}(e^{i\eta_\epsilon}C+e^{-i\eta_\epsilon}D),\\ Be^{ik_hL}&=e^{-2\pi i\varphi}(e^{-i\eta_\epsilon}C+e^{i\eta_\epsilon}D),\\ Ae^{ik_ed_S}&=e^{(ik_F-\lambda_\epsilon)d_S}e^{i\eta_\epsilon}C+e^{(ik_F+\lambda_\epsilon)d_S}e^{-i\eta_\epsilon}D,\\ Be^{ik_hd_S}&=e^{(ik_F-\lambda)d_S}e^{-i\eta_\epsilon}C+e^{(ik_F+\lambda)d_S}e^{i\eta_\epsilon}D.\end{aligned} \tag{A3}$$

The continuity of the derivatives is automatically satisfied in the quasiclassical approximation $\epsilon\ll E_F$. In this approximation, there is no mixing between excitations around $+k_F$ and excitations around $-k_F$. For this reason, it was possible to consider only solution oscillating around $+k_F$ in the ansatz [Eqs. (A1) and (A2)]. The determinant of the system [Eq. (A3)] gives the eigenvalue equation:

$$2i\sin 2\eta_\epsilon\cos k_FL=e^{2\pi i\varphi-i(\epsilon d_N/\hbar v_F)}\sinh(\lambda d_S+2i\eta_\epsilon)-\text{c.c.}, \tag{A4}$$

which is identical to the spectrum obtained by BK:

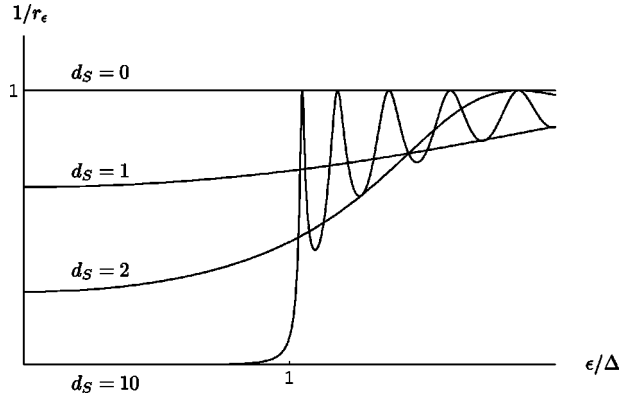

FIG. 13. $1/r_\epsilon$ as a function of energy for different values of d_S in units of ξ_o.

$$\cos k_F L \sin 2\eta_\epsilon = \sin 2\eta_\epsilon \cosh \lambda_\epsilon d_S \cos\left(\frac{\epsilon d_N}{\hbar v_F} - 2\pi\varphi\right) - \cos 2\eta_\epsilon \sinh \lambda_\epsilon d_S \sin\left(\frac{\epsilon d_N}{\hbar v_F} - 2\pi\varphi\right).$$

This formula can be reduced in the following form:

$$\cos k_F L = r_\epsilon \cos\left(\frac{\epsilon d_N}{\hbar v_F} - 2\pi\varphi + \Theta_\epsilon\right), \tag{A5}$$

with the parameters r_ϵ and Θ_ϵ defined by

$$r_\epsilon e^{i\Theta_\epsilon} = \frac{\sinh(2i\eta_\epsilon - \lambda_\epsilon d_S)}{\sinh 2i\eta_\epsilon} \tag{A6}$$

$$= \cosh \lambda_\epsilon d_S + i \cot 2\eta_\epsilon \sinh \lambda_\epsilon d_S. \tag{A7}$$

One expression for the modulus r_ϵ is

$$r_\epsilon = |\cosh \lambda_\epsilon d_S + i \cot 2\eta_\epsilon \sinh \lambda_\epsilon d_S|, \tag{A8}$$

and the phase Θ_ϵ satisfies

$$\tan \Theta_\epsilon = \cot 2\eta_\epsilon \tanh \lambda_\epsilon d_S. \tag{A9}$$

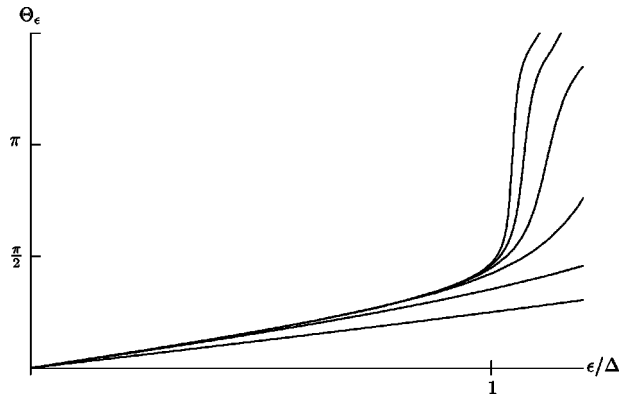

FIG. 14. Phase shift Θ_ϵ as a function of energy for different values of d_S. The curves correspond to $d_S = 1,2,4,6,8,10$ in units of ξ_o from bottom to top. For $d_S \to \infty$, $\Theta_\epsilon \to \pi/2 - \arccos(\epsilon/\Delta)$.

We now look for quasiparticle states with energies above Δ. In the normal region, the form of the wavefunctions is unchanged. In the superconductor, they become

$$\begin{pmatrix} u(x) \\ v(x) \end{pmatrix} = C \begin{pmatrix} e^{-\delta_\epsilon} \\ e^{\delta_\epsilon} \end{pmatrix} e^{i(k_F - \delta k_\epsilon)x} + D \begin{pmatrix} e^{\delta_\epsilon} \\ e^{-\delta_\epsilon} \end{pmatrix} e^{i(k_F + \delta k_\epsilon)x}, \tag{A10}$$

where $e^{2\delta_\epsilon} = (\epsilon + \sqrt{\epsilon^2 - \Delta^2})/\Delta$. Therefore, the eigenvalue equation can be obtained directly from the preceding study with the replacement $-i\eta_\epsilon \to \delta_\epsilon$ and $\lambda \to i\delta k_\epsilon$. We obtain the Eq. (A5) with the complex parameter

$$r_\epsilon e^{i\Theta_\epsilon} = \frac{\sinh(i\delta k_\epsilon d_S + 2\delta_\epsilon)}{\sinh 2\delta_\epsilon} \tag{A11}$$

$$= \cos \delta k_\epsilon d_S + i \coth 2\delta \sin \delta k_\epsilon d_S. \tag{A12}$$

The modulus is given by

$$r_\epsilon = |\cos \delta k_\epsilon d_S + i \coth 2\delta \sin \delta k_\epsilon d_S|, \tag{A13}$$

and the phase by

$$\tan \Theta_\epsilon = \coth 2\delta_\epsilon \tan \delta k_\epsilon d_S. \tag{A14}$$

Equations (A13) and (A14) can be obtained directly from Eqs. (A8) and (A9) by prolongation to energies $\epsilon > \Delta$. The functions r_ϵ and Θ_ϵ are plotted in Figs. 13–15) for different values of d_S. We note that $r_\Delta e^{i\Theta_\Delta} = 1 + i d_S/\xi_o$. We have seen in Sec. II C that these functions have simple limits for very large and for very small d_S/ξ_o.

APPENDIX B: SUPERCURRENT IN SHORT SNS JUNCTIONS

In the case of short SNS junctions, the eigenvalue equation Eq. (44) can be inverted. For the $j=1$, we obtain $\epsilon = \Delta \cos 2\pi y$ in the interval $-1/2 < y < -1/4$ and for $j = -1$, we have $\epsilon = -\Delta \cos 2\pi y$ in the interval $0 < y < 1/4$. These functions $\epsilon^j(y)$ are shown in Fig. 16. Now, we detail

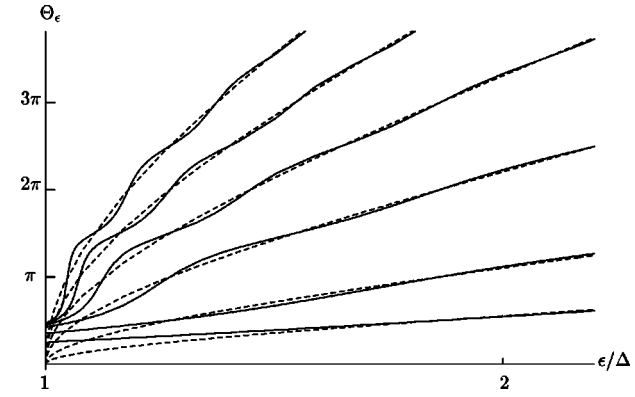

FIG. 15. Asymptotic behavior of Θ_ϵ above Δ for different values of d_S. The curves correspond to $d_S = 1$, 2, 4, 6, 8, and 10 in units of ξ_o from bottom to top. At large energies, Θ_ϵ is close to $\delta k_\epsilon d_S$ which is represented in dashed lines for each value of d_S.

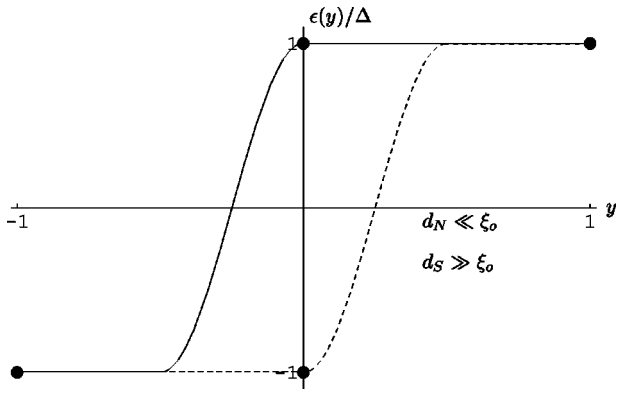

FIG. 16. $\epsilon^j(y)$ for $j=+1$ (solid line) and $j=-1$ (dashed line) $d_S=\infty$, $d_N=0$.

the calculation of the current for the $j=1$ case. From Eq. (33), we get

$$I_m^{j=1}=\frac{4\Delta}{\phi_o}\frac{1}{m}\left[\cos\frac{\pi m}{2}+2\pi\int_{-1/2}^{-1/4}dy\cos 2\pi my\cos 2\pi y\right]. \tag{B1}$$

Odd harmonics with $m\geqslant 3$ are zero. Even harmonics $m=2p$ are

$$I_{2p}^{j=1}=\frac{4\Delta}{\phi_o}(-1)^p\frac{2p}{4p^2-1}. \tag{B2}$$

A similar calculation for $j=-1$ gives the same result for I_m when $m\geqslant 2$. The case $m=1$ has to be considered separately and it is easy to see that $j=+1$ and $j=-1$ cancel each other. Consequently, the current is given by

$$I(\phi)=\frac{4\Delta}{\phi_o}\sum_{p=1}^{\infty}(-1)^p\frac{p}{p^2-1/4}\sin 4\pi p\,\phi/\phi_o, \tag{B3}$$

which is nothing but the harmonics expansion of Eq. (46).

APPENDIX C: EXACT CALCULATION OF THE PERSISTENT CURRENTS IN A NORMAL LOOP

In this appendix, we show how the method developed in Sec. III to calculate the harmonics of the current can be used to obtain the current of the purely normal ring. In this case, it is easier to use the equilibrium single particle state spectrum rather than the excitation spectrum. For a free electron in a ring of length L, the electronic levels are

$$\epsilon_n(\phi)=\frac{2\pi^2\hbar^2}{m_{el}L^2}(n+\varphi)^2. \tag{C1}$$

The derivation of Eq. (33) is still valid for the equilibrium spectrum:

$$I_m(T=0)=\frac{4}{\pi m}\frac{1}{\phi_o}\left[\frac{d\epsilon}{dy}(y_F)\cos 2\pi my_F-\int_0^{y_F}dy\frac{d^2\epsilon}{d^2y}\cos 2\pi my\right]. \tag{C2}$$

We have added an additional factor 2 for the spin degeneracy. The first term in Eq. (C2) gives the above result [Eq. (43)], but the second term gives a nonvanishing correction due to the parabolic dispersion relation. This correction is easy to evaluate since the curvature $d^2\epsilon/d^2y=4\pi^2\hbar^2/m_{el}L^2$ is a constant and we obtain

$$\delta I(\phi)=-\frac{4}{\pi}\frac{ev_F}{L}\frac{1}{k_FL}\sum_{m=1}^{\infty}\frac{\sin mk_FL}{m^2}\sin 2\pi m\phi/\phi_o, \tag{C3}$$

which is the $1/k_FL$-corrective term to the zeroth order term obtained in Eq. (43).

[1] M. Büttiker and T.M. Klapwijk, Phys. Rev. B **33**, 5114 (1986).

[2] A.F. Andreev, Zh. Éksp. Teor. Fiz. **46**, 1823 (1964) [Sov. Phys. JETP **19**, 1228 (1964)].

[3] J. Bardeen and J.L. Johnson, Phys. Rev. B **5**, 72 (1972).

[4] C. Ishii, Prog. Theor. Phys. **44**, 1525 (1970).

[5] A.V. Svidzinskii, T.N. Antsygina, and E.N. Bratus, Zh. Éksp. Teor. Fiz. **61**, 1612 (1971) [Sov. Phys. JETP **34**, 4 (1972)].

[6] I.O. Kulik and A.N. Omel'yanchuk, Fiz. Nizk. Temp. **3**, 945 (1977) [Sov. J. Low Temp. Phys. **3**, 459 (1977)]; **4**, 296 (1978) [**4**, 142 (1978)].

[7] C.W.J. Beenakker and H. van Houten, Phys. Rev. Lett. **66**, 3056 (1991).

[8] J. Bardeen, R. Kümmel, A.E. Jacobs, and L. Tewordt, Phys. Rev. **187**, 556 (1969).

[9] C.W.J. Beenakker and H. van Houten, in *SQUID'91*, edited by H. Koch and H. Lübbig (Springer-Verlag, Berlin, 1991).

[10] P. G. de Gennes, *Superconductivity of Metals and Alloys* (Benjamin, New York, 1966).

[11] The results obtained in this paper depend on the parity of the number N of electrons per spin direction. The total number of electrons $2N$ is always even throughout this paper.

[12] We choose to define the superconductor coherence length by $\xi_o=\hbar v_F/\Delta$ for convenience, instead of the usual definition $\xi_o=\hbar v_F/\pi\Delta$.

[13] F. Bloch, Phys. Rev. **137**, A787 (1965); **166**, 415 (1968).

[14] I.O. Kulik, Zh. Éksp. Teor. Fiz. **57**, 1745 (1969) [Sov. Phys. JETP **30**, 944 (1970)].

[15] P.F. Bagwell, Phys. Rev. B **46**, 12573 (1992).

[16] P. Samuelsson, J. Lantz, V.S. Shumeiko, and G. Wendin, Phys. Rev. B **62**, 1319 (2000).

[17] We use the usual convention for the current in a loop, namely positive if the current is paramagnetic. Our result differs from the BK one by a factor of 4. We think that our prefactor is right result because it leads to the normal ring result for $d_S\to 0$. The

harmonics expansion follows directly from the application of our formalism, while in the work of BK it was constructed by analogy with the long SNS junction result.

[18] H.F. Cheung, Y. Gefen, E.K. Riedel, and W.H. Shih, Phys. Rev. B **37**, 6050 (1988).

[19] K.K. Likharev, Rev. Mod. Phys. **51**, 101 (1979).

[20] H. Bouchiat and G. Montambaux, J. Phys. (Paris) **50**, 2695 (1989).

[21] H.F. Cheung, Y. Gefen, and E.K. Riedel, IBM J. Res. Dev. **32**, 359 (1988).